Drag Reduction Phenomenon in Viscous Oil-Water Dispersed Pipe Flow: Experimental Investigation and Phenomenological Modeling

I. H. Rodriguez, H. K. B. Yamaguti, and M. S. de Castro
Dept. of Mechanical Engineering, Engineering School of Sao Carlos, University of Sao Paulo (USP), São Carlos, SP 13566-970, Brazil

M. J. Da Silva
Forschungszentrum Dresden-Rossendorf e. V., Institute of Safety Research, Dresden 01314, Germany

O. M. H. Rodriguez
Dept. of Mechanical Engineering, Engineering School of Sao Carlos, University of Sao Paulo (USP), São Carlos, SP 13566-970, Brazil

DOI 10.1002/aic.12787
Published online October 25, 2011 in Wiley Online Library (wileyonlinelibrary.com).

An experimental study on drag-reduction phenomenon in dispersed oil-water flow has been performed in a 26-mm-i.d. Twelve meter long horizontal glass pipe. The flow was characterized using a novel wire-mesh sensor based on capacitance measurements and high-speed video recording. New two-phase pressure gradient, volume fraction, and phase distribution data have been used in the analysis. Drag reduction and slip ratio were detected at oil volume fractions between 10 and 45% and high mixture Reynolds numbers, and with water as the dominant phase. Phase-fraction distribution diagrams and cross-sectional imaging of the flow suggested the presence of a higher amount of water near to the pipe wall. Based on that, a phenomenology for explaining drag reduction in dispersed flow in a flow situation where slip ratio is significant is proposed. A simple phenomenological model is developed and the agreement between model predictions and data, including data from the literature, is encouraging. © 2011 American Institute of Chemical Engineers *AIChE J,* 58: 2900–2910, 2012
Keywords: liquid–liquid flow, oil-water flow, dispersed flow, drag reduction, phenomenological modeling, wire-mesh sensor

Introduction

The common occurrence of multiphase flows in pipes has motivated much research interest in this field. Liquid–liquid flow is commonly encountered in the petroleum industry, where a number of applications involve oil-water flow such as crude oil production and transportation. The water proportion in crude oil production is increasing day by day and then the flow of oil-water mixtures is receiving more attention from the researchers. In oil transportation process the flow of a mixture of oil and water through pipelines over long distances causes significant pressure losses. The cocurrent pipe flow of two liquids is more complex as compared to single-phase flow of either of the fluids and the prediction of the frictional pressure gradient usually cannot be made by extrapolation of single-phase codes. The proper design of a two-phase production well or pipeline depends on the accurate prediction of this frictional pressure gradient. This has been one of the main reasons behind the great interest in the study of oil-water flows observed in recent years.

Correspondence concerning this article should be addressed to I. H. Rodriguez at iarahr@sc.usp.br.

The dispersed flow pattern, where one phase is dispersed as droplets into the other continuous phase, is common in crude oil transmission and offshore pipelines, with either oil or water as the dominant phase. However, it has not been studied as intensively as separated or intermittent flows. An interesting feature of liquid–liquid flow is the drag reduction phenomenon (DRP), yet not well understood. The occurrence of DRP without the addition of drag reduction agents in dispersed flow has been reported in some previous studies. Drag reduction phenomenon can be defined as a reduction in two-phase pressure gradient in comparison with single-phase equivalent values.

Pal[1] investigated the behavior of oil-water dispersions and emulsions in laminar and turbulent horizontal flows. He found that such dispersions exhibit drag reduction in turbulent flow. The effective viscosity values obtained in turbulent flow are smaller than the equivalent values in laminar flow. This indicates a relative decrease of the pressure gradient in turbulent regime. He believes that in turbulent pipe flow of dispersions the deformation of drops could cause the modification of the turbulence scales of the continuous phase flow, which could explain the DRP associated to oil-water dispersed flows. In addition, he indicates that the intensity of the drag reduction depends on the oil physical properties and

on the concentration of the dispersed phase. Moreover, the author proposed a theoretical method to predict the viscosity of emulsions of two immiscible liquids, based on the effective rheological properties of the mixture. The proposed equation predicts the viscosity data of emulsions very well, covering a broad range of viscosity values.[2]

Nädler and Mewes[3] investigated the flow of oil and water in a horizontal pipe made of perspex with an inner diameter of 59 mm and a total length of 48 m. Those authors observed drag reduction in oil-in-water dispersion and in a flow pattern that consisted of a water layer and layers of dispersion of water-in-oil and oil-in-water. The minimum two-phase pressure drop was of the order of that of pure water flowing alone in the pipe at the same mixture superficial velocity. Angeli and Hewitt[4] measured pressure gradients in oil-water flow with a low viscosity oil in two horizontal 25.4-mm-i.d. pipes made from stainless steel and acrylic resin. They found that the two-phase pressure gradient and phase distribution depend strongly on the pipe material and attribute it to wettability effects of the pipe wall. A drag reduction was observed at high mixture velocities (2.6–3.0 m/s) and low water fraction, where the dispersed pattern prevails (being the oil the continuous phase) in both pipes. Experimental mixture friction factors were measured with either oil or water as continuous phases and also in single phase flows. The mixture friction factors were significantly smaller than the single phase ones when the oil is the continuous phase and almost the same when the water is the continuous phase.

Some other authors also observed lower pressure gradients than those of single-phase water flow during oil-water dispersed or semidispersed flow in horizontal pipes. Lovick and Angeli[5] and Ioannou et al.[6] detected drag reduction and slip ratio in dispersed and dual continuous flows. They do not explain the drag reduction, but argue that the slip ratio could be explained in the light of the momentum balance between the separated phases. It could make sense for the dual continuous flow, but does not explain the slip ratio observed in fully dispersed flow patterns. Lum et al.[7] found that the two-phase pressure gradient takes values below the single phase water one in upward and downward pipe inclinations at high mixture velocities and high oil fractions.

It is interesting to note that the drag reduction in oil-water dispersed flow has been detected by a few researchers, but the underlying physical mechanism behind the phenomenon is still not well understood. Pal[8] proposed a mechanism for the modeling of DRP in turbulent oil-in-water and water-in-oil dispersions. Based on the mixture effective rheological aspects, the phenomenon in oil-water dispersions would be caused by a significant reduction of the effective viscosity of the dispersion when the flow regime passes from laminar to turbulent. The author believes that the drag reduction observed in turbulent flow is caused by the decrease of the mixture effective viscosity and this in turn is caused by the deformation of droplets of the dispersed phase and the decrease of interfacial tension. According to the author, the dispersion or emulsion would be a non-Newtonian fluid and by modeling its rheology it would be possible to predict the drag reduction.

The existence of a thin laminar film flow adjacent to the pipe wall and surrounding a viscous phase has been the explanation for very low frictional pressure gradients observed in liquid–liquid pipe flow. In two-phase pipe flow of immiscible liquids the core-annular flow pattern, in which the thicker fluid is surrounded by the thinner one, is commonly observed when the conditions are such that both fluids form continuous and parallel phases. A very interesting feature of this flow configuration is that the frictional pressure drop is comparable or even lower to that of the single-phase flow of the thinner fluid under equivalent flow conditions—see, for example, Refs. 9 and 10. The pioneer studies of Russel and Charles[11] and Charles et al.[12] for horizontal pipes showed that this flow pattern occurs when the two liquids have similar densities and relatively small quantities of water are added. Ooms,[13] Ooms et al.,[14] and Oliemans[15] showed that for the existence of core-annular flow the annulus must be thin and there must be asymmetric interfacial waves. These authors proposed the 'Lubrication theory for core-annular flow.' Joseph et al.[16] and Feng et al.[17] studied the hydrodynamic stability of two immiscible liquids flowing in a pipe, showing that the more viscous fluid must occupy most of the pipe's cross-section and that asymmetric interfacial waves would be responsible for the levitation of the core phase. The inclusion of the inertial terms characterized the Levitation theory for core-annular flow. Bai,[18] Bai et al.,[19] and Bai and Joseph[20] carried out experimental works and numerical simulations for upward vertical core-annular flow and presented results on two-phase pressure drop and interface shape. Rodriguez and Bannwart[21,22] offered detailed experimental data and proposed an analytical solution for the interfacial waves in upward-vertical core-annular flow. Recently, Rodriguez et al.[23] proposed a more refined pressure-loss model for core-annular flow, including a slip ratio term that implicitly accounts for the buoyancy of the oil core, and Rodriguez and Bannwart,[24] using the 1-D two-fluid model, showed that the prediction of flow-pattern transition can be significantly improved if new critical wave numbers are incorporated in the transition criteria.

In that context, one may notice that the experimental investigation of liquid–liquid flows, especially oil-water flow, is growing because of the industrial relevance. However, more research into the physics of liquid–liquid flow is necessary. As a consequence, a considerable number of different measurement techniques for liquid–liquid flows have been proposed. Electrical capacitance tomography is of great interest because it is low cost, noninvasive and nonintrusive and can achieve good temporal resolution; however, it offers low spatial resolution due to the intrinsic limitation of the soft-field method and the nonlinear relationship between electrical measurements and the permittivity of the measured material.[25,26] On the other hand, hard-field methods as single or multibeam gamma-ray densitometry offer good spatial resolution and are also noninvasive and nonintrusive, but are expensive, radioactive and have poor temporal resolution due to the relatively long counting times required for the statistics.[27–29] Optical techniques as laser Doppler anemometry or particle image velocimetry (PIV) are nonintrusive and non invasive and have high spatial and temporal resolutions, but are relatively expensive and require a transparent medium and a transparent pipe material, which practically limits the methods to the laboratory environment.[30] Attempts to combine in a single measurement technique high temporal and spatial resolutions, field application, safety and low cost is in order.

The wire-mesh sensor based on conductivity measurements, introduced about 10 years ago by Prasser et al.[31] is a hybrid method in the sense that it combines intrusive local measurement of phase fraction and tomographic cross-

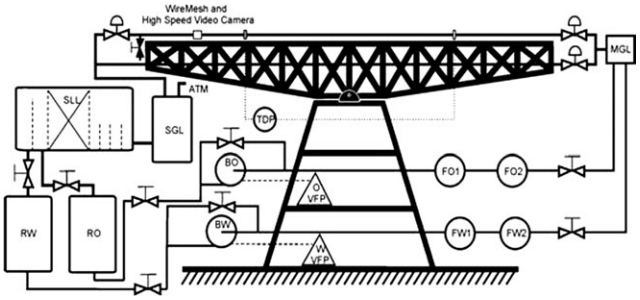

Figure 1. Schematic view of the multiphase flow loop.

sectional imaging with good spatial resolution (up to 1 mm) and high temporal resolution. In this study we used the wire-mesh sensor based on measurements of electrical permittivity (capacitance) that has been recently developed by Da Silva.[32] The permittivity measurements overcame the limitation of the wire-mesh sensor for investigating flows involving nonconducting fluids, such as oil-air flow. The disadvantage of being invasive is in part compensated by a better spatial resolution, the high temporal resolution, low cost and simplicity when compared with other tomography systems. Rodriguez et al.[33] applied for the first time the capacitive wire-mesh sensor for the study of viscous oil-water flow and showed that for a flow dominated by turbulence it can be an accurate and reliable tool.

The drag reduction effect has been reported by few researchers in low viscosity oil-water dispersed flow. Nevertheless, the physical mechanism, to the authors' knowledge, has never been properly explained. Therefore, the main aim of this article is the proposition of a phenomenology for explaining drag reduction in a flow situation where slip ratio is significant. New data on dispersed viscous oil-water flow were collected to supplement the scanty information available in the literature. Based on experimental evidence provided by a novel capacitive wire-mesh sensor, a phenomenological model is proposed. This article is structured as follows: the 'Experimental work' section describes the experimental device, instrumentation, and measurement techniques; the 'Experimental Results and Discussion' section shows the experimental results, pressure gradient, friction factor, volume fractions, and phase distribution; the 'Modeling' section describes the model, and in the 'Results' section the predictions are discussed. The 'Conclusion' section summarizes the main results.

Experimental Work

Experimental set-up

The experiments reported in this article were performed in the Thermal-Fluids Engineering Laboratory of the Engineering School of São Carlos, University of São Paulo. The multiphase-flow loop is shown schematically in Figure 1. The main instruments of the facility are described in Table 1. The test section consists of a glass line of 26-mm-i.d. and 12-m-length. A by-pass line allowed the usage of the quick-closing-valve (QCV) technique to measure the *in situ* volume fraction of the phases. The test fluids, water and oil (860 kg/m^3 of density and 100 mPa s of viscosity) were kept in polyethylene tanks, (RW) and (RO), respectively. Positive displacement water and oil pumps (BW and BO, respectively), both remotely controlled by their respective variable-frequency drivers, pumped the phases to the test line. Oil and water joined at the beginning of the test section via a Y-junction. Positive displacement and vortex flow meters (FO1, FO2, FW1, FW2) were used to measure the flow rates of the fluids. After the test section the oil-water mixture flows to a coalescent-plate liquids separator tank (SLL), where gravitational separation of the two liquids is obtained. Once separated, oil and water return to their respective storage tanks, (RO) and (RW).

The dispersed flow was identified by visual observation using a high-speed video camera (Optronis, Camrecord 600). A projected lateral view of the flow was recorded through a Perspex visualization section located at 10.3 m from the tube entrance (Figure 2c). The recording speed was 2000 frames per second.

In situ phase volume fractions were obtained from the QCVs with an experimental uncertainty ranging from $\pm 0.88\%$ to $\pm 2.58\%$.[33] The valves were placed at each end of the glass pipe, with a trapped liquid volume of 6400 ml. Moreover, the data of oil volume fraction from the QCVs was compared with those obtained using the wire-mesh sensor based in capacitance measurements, showing an average relative error for all conditions of 16.3%.

The prototype of the wire-mesh sensor was also used to obtain phase-fraction distribution diagrams and cross-sectional images of the flow. The prototype consisted of two cross-sectional planes made of eight stainless steel wires of 0.12-mm diameter evenly distributed over the 26.2-mm pipe diameter, 3 mm of wire separation on each cross-sectional plane, which also determines the spatial resolution of the instrument, and 1 mm of axial plane separation (Figure 2a).

Table 1. Main Instruments and Equipment of the Facility

	Water variable-frequency driver (WVFP) Oil variable-frequency driver (OVFP)		FO1—oil high flow meter FO2—oil low flow meter FW1—water high flow meter FW2—water low flow meter
	Quick closing valve		Control valve
TDP	Differential pressure transducer		BW—water pump BO—oil pump
SLL	Coalescent-plates liquid–liquid separator		Drainage valve
MGL	Multiphase mixer	RW	Water tank
RO	Oil tank	SGL	Gas-liquid separator tank

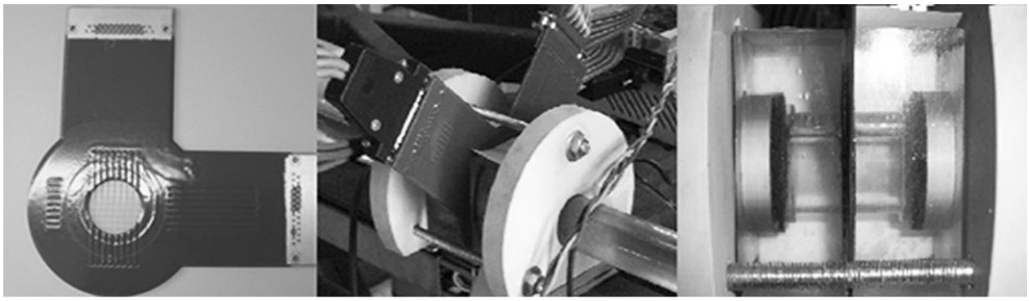

(a) (b) (c)

Figure 2. Wire-mesh used in this study (a) Prototype of the sensor; (b) sensor installed at the test section; (c) visualization section.

The sensor was installed at the end to the horizontal test section (10.3 m from the tube entrance) in between the two halves of the Perspex visualization section. Therefore, it was also possible to observe the effect of the wire-mesh sensor over the flow patterns (Figures 2b, c). The time resolution of the prototype was 500 frames per second. Details about the wire-mesh data processing and principle are described in Da Silva[32] and Rodriguez et al.[33]

The pressure drop was measured in the horizontal glass pipe by a previously calibrated differential pressure transducer (SMAR LD301D) with pressure taps located on the test section at 2.8 and 8.9 m from the pipe inlet, respectively. The temperature of the pipe was monitored during the experiments with a thermocouple. The temperature of the oil was taken into account to evaluate the variation of oil viscosity.

The full set of experimental points is formed by 64 points (a point means a pair of oil and water superficial velocities). Measurements were made for mixture velocities from 0.9 to 4.0 m/s and for oil cuts from 10 to 70%. The entire set of experimental data was used to obtain the pressure drop data. Nevertheless, a set formed by 32 points was used for measurements with the wire-mesh sensor.

Pressure drop measurements

The pressure drop was recorded for a wide range of oil and water flow rates within the region of the flow map predicted as dispersion of oil in water[28] as an attempt to cover the range of occurrence of the DRP. Pressure gradients for the two-phase flow and pressure gradients for related single-phase water flow were collected. The factor used to determine the occurrence of the phenomenon was the ratio between the measured two-phase flow pressure gradient and the measured related single-phase water pressure gradient. The latter refers to the pressure gradient measured in single-phase water flow at the same mixture velocity. This ratio was defined as DRP factor

$$\mathrm{DRP} = \frac{-\left(\frac{dp}{dx}\right)_{\mathrm{m}}}{-\left(\frac{dp}{dx}\right)_{\mathrm{w}}} \tag{1}$$

where $(dp/dx)_{\mathrm{m}}$ and $(dp/dx)_{\mathrm{w}}$ represent the two-phase and single-phase water pressure gradients, respectively. Note that if the mixture pressure gradient is lower than that of water flowing alone in the pipe at the same mixture velocity the DRP factor is <1, which indicates drag reduction.

Experimental Results and Discussions

In Table 2 one can see all the collected experimental data. It contains the slip ratio s, the pressure gradient of the mixture $(dp/dx)_{\mathrm{m}}$, the pressure gradient of water flowing at mixture velocity $(dp/dx)_{\mathrm{w}}$, the water and oil superficial velocities, respectively (U_{ws}, U_{os}), the oil *in situ* volume fractions (*holdup*) measured by the QCV technique (ε_{o}) and the flow pattern. The analysis of the wire-mesh data together with the recorded movies allowed the identification of three different flow patterns: a homogeneous dispersion of oil in water (o/w H), a nonhomogeneous dispersion of oil in water (o/w NH) and a dispersion of oil in water and water in oil (Do/w & Dw/o). The o/w H and o/w NH flow patterns were always water dominated. According to the phase-inversion model of Brauner and Ullmann[34] and for our flow conditions, an oil superficial velocity of at least 5 m/s would be necessary for reaching the predicted phase-inversion boundary. Our maximum oil superficial velocity was of 1 m/s. In addition, the movies (recorded at 2000 fps) always showed oil droplets dispersed in water. The wire-mesh gave the same indication. More details regarding the flow patterns can be seen in Rodriguez et al.[33] Note that $(dp/dx)_{\mathrm{w}}$ is higher than $(dp/dx)_{\mathrm{m}}$ (DRP factor <1) for all data, except for three conditions at the highest superficial water velocity of 3 m/s, namely those for superficial oil velocities of 0.2, 0.5, and 1.0 m/s. Also one can see that the slip ratio is >1 (from 1.03 to 1.20) for all data. It was obtained by the expression $s = (\varepsilon_{\mathrm{w}}/\varepsilon_{\mathrm{o}})/(C_{\mathrm{w}}/C_{\mathrm{o}}) = V_{\mathrm{o}}/V_{\mathrm{w}}$, where ε_{o} and ε_{w} are the experimental *in situ* volume fractions, C_{o} and C_{w} are the cuts and V_{o} and V_{w} are the average velocities of oil and water, respectively. Accordingly, s is >1 when oil is flowing faster, and, conversely, s is <1 when water is flowing faster than oil. The results show that oil is flowing between 3 and 20% faster than water overall, which indicates that either the mixture is not homogeneous or that phase separation occurs. An interesting finding is that even the oil-in-water homogeneous dispersion (o/w H) observed at high mixture Reynolds numbers (about 10^5) presented a slip ratio higher than 1, with oil flowing 8% faster than water on average.

Pressure gradient

Two-phase pressure gradient data normalized with respect to the equivalent single-phase water pressure gradient (pressure gradient at the same mixture velocity) given by the DRP factor is shown in Figure 3 as a function of the oil superficial velocity for water superficial velocities of 1.0,

Table 2. Experimental Data

Run	U_{ws} (m/s)	U_{os} (m/s)	Oil Holdup, ε_o (QCV)	Flow Pattern	Slip Ratio, s	$-(dp/dx)_m$ (Pa/m)	$-(dp/dx)_w$ (Pa/m)
9	3.0	0.2	0.0593	Do/w H	1.06	3862	3477
10	3.0	0.5	0.1359	Do/w H	1.06	4444	4013
52	3.0	0.8	0.2008	Do/w H	1.06	4597	4703
11	3.0	1	0.2339	Do/w H	1.09	5405	5085
43	2.5	0.2	0.0711	Do/w H	1.05	2480	2598
44	2.5	0.3	0.1015	Do/w H	1.06	2610	2734
45	2.5	0.4	0.1292	Do/w H	1.08	2781	2898
46	2.5	0.5	0.1542	Do/w H	1.10	2925	3079
47	2.5	0.6	0.1891	Do/w H	1.03	3080	3265
48	2.5	0.7	0.2016	Do/w H	1.11	3224	3477
49	2.5	0.8	0.226	Do/w H	1.10	3384	3664
50	2.5	0.9	0.2499	Do/w H	1.08	3536	3838
51	2.5	1	0.2729	Do/w H	1.07	3687	4013
29	2.0	0.3	0.1162	Do/w H	1.14	1993	2003
30	2.0	0.4	0.15	Do/w H	1.13	2114	2166
31	2.0	0.6	0.2124	Do/w H	1.11	2311	2469
32	2.0	0.7	0.2411	Do/w H	1.10	2407	2598
33	2.0	0.8	0.2687	Do/w H	1.09	2533	2734
34	2.0	0.9	0.2953	Do/w H	1.07	2656	2898
41	1.5	0.3	0.1602	Do/w NH	1.05	1167	1351
40	1.5	0.4	0.1988	Do/w NH	1.07	1281	1470
39	1.5	0.5	0.2319	Do/w NH	1.10	1439	1591
38	1.5	0.6	0.2609	Do/w NH	1.13	1562	1716
37	1.5	0.7	0.288	Do/w NH	1.15	1694	1818
36	1.5	0.8	0.312	Do/w NH	1.18	1818	2003
35	1.5	0.9	0.3333	Do/w NH	1.20	1922	2166
21	1.0	0.3	0.2188	Do/W & Dw/o	1.07	636	852
22	1.0	0.4	0.2692	Do/W & Dw/o	1.09	803	958
23	1.0	0.5	0.3123	Do/W & Dw/o	1.10	843	1098
24	1.0	0.6	0.3492	Do/W & Dw/o	1.12	975	1131
25	1.0	0.7	0.3813	Do/W & Dw/o	1.14	1089	1236
26	1.0	0.8	0.4091	Do/W & Dw/o	1.16	1220	1351
28	1.0	0.9	0.4335	Do/W & Dw/o	1.18	1352	1470

1.5, 2.0, 2.5, and 3.0 m/s. The measurements were made for input oil fractions (oil cut) varying from 10 to 40%.

In Figure 3, the dashed line indicates Do/w & Dw/o and solid lines indicate o/w H and o/w NH. DRP-factor values <1 were observed at water superficial velocities ranging from 1 to 2.5 m/s, which indicates a decrease in two-phase pressure gradient in comparison with related single-phase water values. In addition, they tend to converge to the value of about 0.9 with increasing the oil superficial velocity. However, the same behavior was not observed at the highest water velocity (3 m/s). A maximum drag reduction of up to 25% was detected ($U_{ws} = 1$ m/s) and on average it was of 0.93%. The experimental uncertainties of the measured two-phase and related single-phase water pressure gradients were estimated to be ranged from $\pm 0.21\%$ to $\pm 1.28\%$ and from $\pm 0.2\%$ to $\pm 1.72\%$, respectively.[33]

Friction factor and effective viscosity estimates

The homogeneous model[35] is commonly used for dispersed flows to predict the frictional pressure gradient. In such model the two-phase flow is treated as a mixture that is considered as a single fluid with averaged physical properties and the assumption of no-slip is assumed. Thus, the mixture density, ρ_m, is given by

$$\rho_m = \rho_o C_o + (1 - C_o)\rho_w \tag{2}$$

in which

$$C_o = \frac{U_{os}}{U_{ws} + U_{os}} \tag{3}$$

where C_o is the oil cut, ρ_w and ρ_o and U_{ws} and U_{os} are water and oil densities and superficial velocities, respectively. It is important to note that in the homogeneous no-slip model the oil cut is equal to the oil *in situ* volume fraction.

Provided the flow is fully dispersed, the mixture friction factor is given by

$$f_m = -\left(\frac{dp}{dx}\right)_m \frac{2D}{\rho_m U_{ms}^2} \tag{4}$$

where $(dp/dx)_m$ is the mixture pressure gradient, U_{ms} is the mixture velocity ($U_{ms} = U_{ws} + U_{os}$) and D is the pipe's internal diameter. Similarly, single-phase water friction factor was predicted by

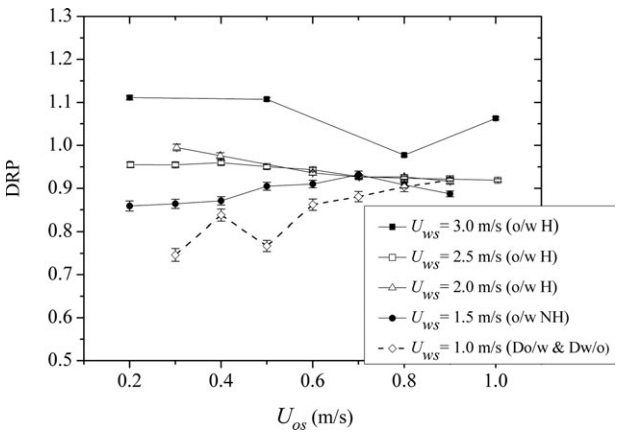

Figure 3. DRP factor against oil superficial velocity at different water superficial velocities.

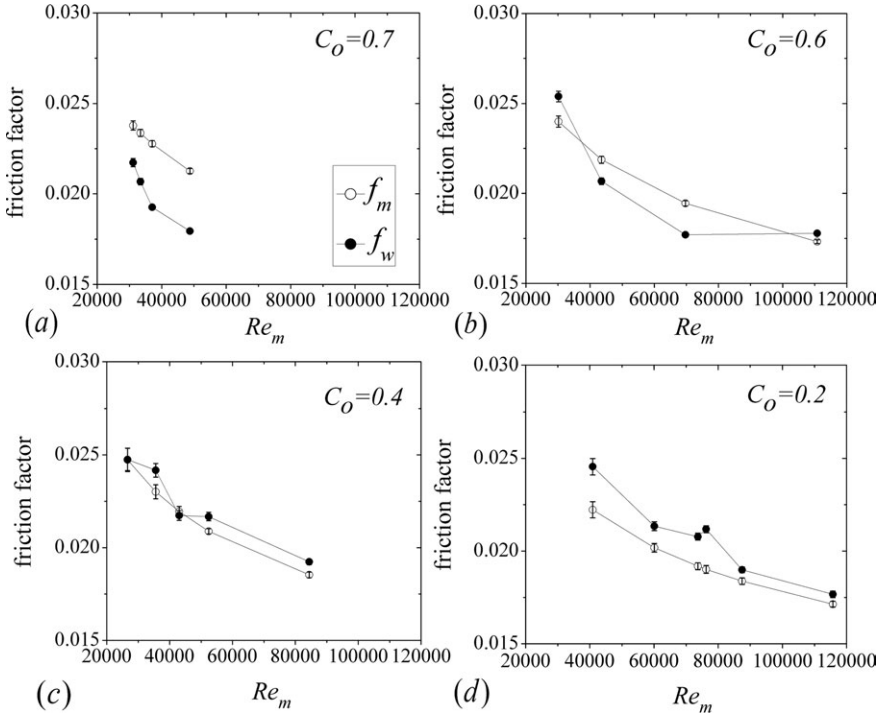

Figure 4. Mixture and related water friction factors against mixture Reynolds number for different oil cuts.

$$f_w = -\left(\frac{dp}{dx}\right)_w \frac{2D}{\rho_w V^2} \quad (5)$$

where $(dp/dx)_w$ stands for single-phase water pressure gradient, V is the water mean velocity. Note that for each experimental point $V = U_{ms}$.

In dispersed flow, making predictions of pressure gradient asks for the validation of an effective viscosity model. The effective viscosity of the mixture, μ_m, is needed for calculating the mixture Reynolds number

$$Re_m = \rho_m U_{ms} D/\mu_m \quad (6)$$

and can be estimated by using the measured pressure gradients.[36] In the present study, friction factor correlations of single-phase flow have been applied for the oil-water dispersed flow. The mixture friction factor, f_m, is given by Blasius relation for a smooth tube, $f_m = b.Re_m^{-n}$, where the parameters b and n are assumed to be $b = 0.3164$ and $n = 0.25$ for $Re_m < 10^5$ and $b = 0.184$ and $n = 0.2$ for $Re_m > 10^5$.[35] Based on that, the effective viscosity can be determined by solving Eq. 4 with Blasius relation for each measurement. The results are shown in Figures 4 and 5. The experimental mixture and related single-phase water friction factors were plotted against the mixture Reynolds number for four different oil fractions (Figure 4). The mixture Reynolds numbers ranged from 30,000 to 120,000. At the highest oil volume fraction (70%) the mixture friction factor was higher than that of single-phase water flow (Figure 4a). At 60% of oil fraction (Figure 4b) a trend of crossing between the lines is observed. At lower oil volume fractions, 20 and 40% (Figures 4c, d), the single-phase water friction factor is higher than the mixture friction factor. These results also show that in dispersions of oil in water the drag reduction occurs at low oil fractions.

The effective viscosity results are displayed in Figure 5. The mixture viscosity was found to be lower than the water viscosity (0.001 Pa s) for water cuts higher than 50%. These results suggest once more the occurrence of a drag reduction in oil-in-water dispersed flow at low oil fractions.

Volume fraction and phase distribution

A comparison between the oil volume fraction measured by the QCVs and that predicted by the homogeneous model showed that the model overestimates the experimental data. The oil fraction predicted by the homogenous model was always higher than that measured by the QCVs, which indicates that the oil is the flowing fastest phase and the no-slip condition is not satisfied. The average relative deviation between data and predictions of the homogeneous model was of 7.78%. The experimental uncertainty of the oil fraction measured by the QCVs was estimated to be ranged from ±0.88% and ±2.58%. Also, two permittivity models were applied to measure the oil fraction using the wire-mesh sensor. The results were compared with the oil volume fraction data measured by the QCVs and quite good agreement was

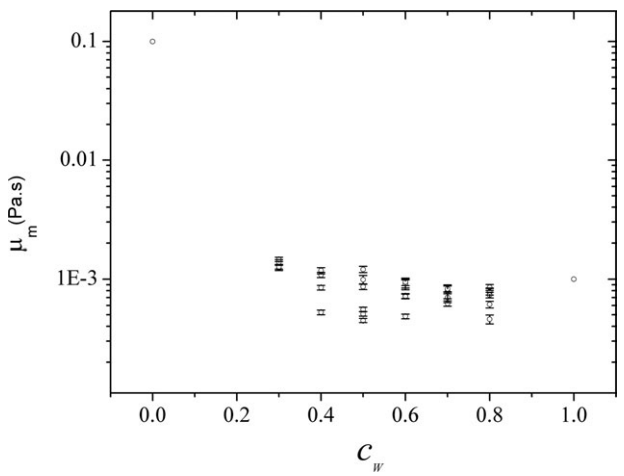

Figure 5. Mixture viscosity against water cut.

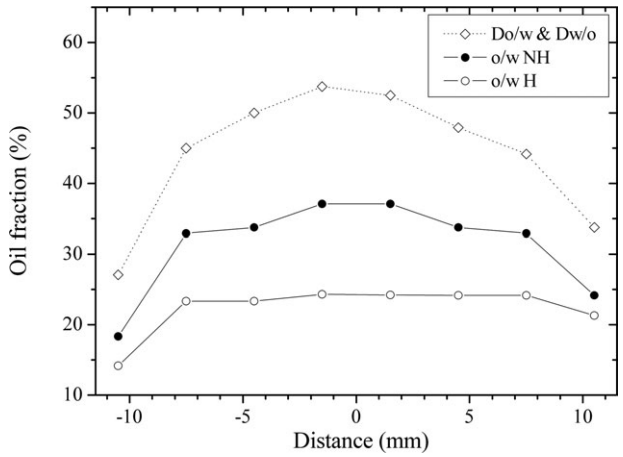

Figure 6. Vertical chordal time-averaged oil fraction distribution going from left to right over the pipe's cross section for the three flow patterns observed.

o/w H (U_{ws} = 2.5 m/s, U_{os} = 0.8 m/s), o/w NH (U_{ws} = 1.5 m/s, U_{os} = 0.8 m/s), and Do/w & Dw/o (U_{ws} = 1.0 m/s, U_{os} = 0.8 m/s).

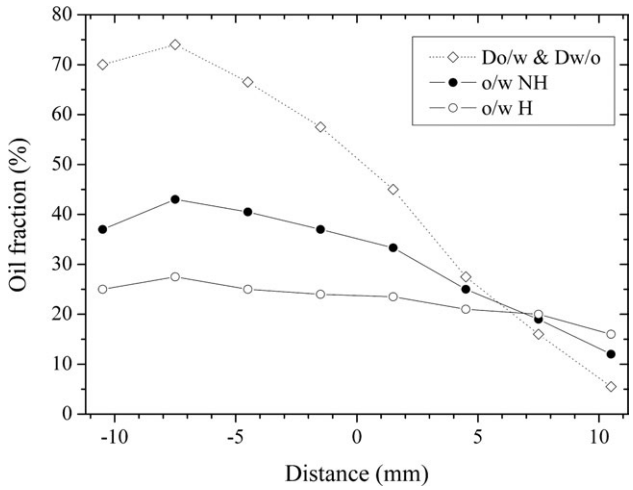

Figure 7. Horizontal chordal time-averaged oil fraction distribution going from top to bottom over the pipe's cross section for the three flow patterns observed.

o/w H (U_{ws} = 2.5 m/s, U_{os} = 0.8 m/s), o/w NH (U_{ws} = 1.5 m/s, U_{os} = 0.8 m/s), and Do/w & Dw/o (U_{ws} = 1.0 m/s, U_{os} = 0.8 m/s). (negative distances: above the pipe centerline; positive distances: below the pipe centerline).

observed. The average relative error of the oil fraction measured by the Maxwell-Garnett model and Logarithmic model in comparison to that measured by the QCVs was of 16.3% and 5.8%, respectively (for details see Rodriguez et al.[33]).

Oil fraction distributions obtained by the wire-mesh sensor are shown in Figures 6 and 7 for three typical experimental points corresponding to the three flow patterns observed at the flow conditions investigated: o/w H (U_{ws} = 2.5 m/s, U_{os} = 0.8 m/s), o/w NH (U_{ws} = 1.5 m/s, U_{os} = 0.8 m/s), and Do/w & Dw/o (U_{ws} = 1.0 m/s, U_{os} = 0.8 m/s). Chordal oil fraction distributions were obtained for each condition by averaging the local oil fractions in time and in vertical or horizontal chords over the cross-section. Vertical and horizontal chordal oil fraction distributions can be seen in Figures 6 and 7, respectively. In Figure 6, the phase distribution data indicate that even the homogeneous dispersion of oil in water (**o/w H**), where the oil should be evenly dispersed over the cross-section, presents a decrease of oil fraction near to the pipe wall.

For the dual continuous flow (Do/w & Dw/o), where both phases form continuous layers separated by a turbulent interface, one would expect the less dense phase (oil) to occupy the top of the pipe, i.e., it is not expected to exist any fraction of water at the top of the pipe. However, in Figure 7 at about distance −10 mm from the pipe centerline the trend change suggests the presence of water at the top of the pipe, even for the Do/w & Dw/o. Figures 6 and 7 suggest the existence of an amount of water near to the pipe wall for all flow patterns. Notice that Figures 6 and 7 are important only for inquiring the trend of the local oil fraction distribution, which is not affected by slight changes in the values of the time-averaged oil fraction. Hence, error bars are not considered necessary in Figures 6 and 7.

In Figure 8 one can see the cross-sectional phase distribution diagram also obtained by the wire-mesh sensor. At the lowest water superficial velocity, where Dual Continuous flow was observed (Figure 8c), the topmost layer seems to have a significant fraction of water. At intermediate water superficial velocity, Nonhomogeneous dispersion was seen and a similar trend was observed, but in this case oil and water are not forming an interface (Figure 8b). At the highest water superficial velocity (Figure 8a), an increase of the water fraction at the top of the pipe is still noted even though the phase distribution is practically uniform at this flow conditions.

One may argue that the wire-mesh delivers only qualitative results. On the other hand, the measurements have shown with a good degree of certainty that at about 5 mm from the pipe wall there was a significant increase of the water fraction, even at the top of the pipe (Figures 6–8). The

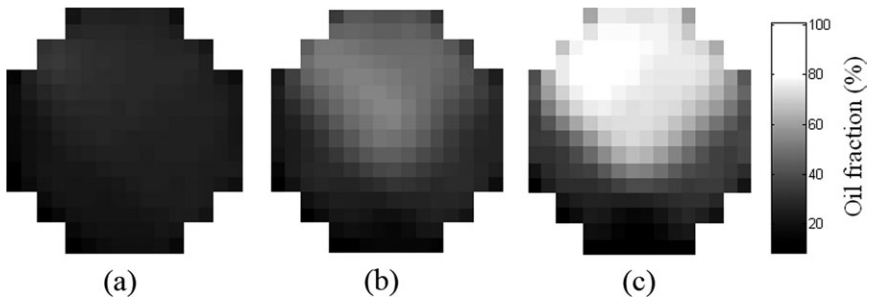

Figure 8. Cross sectional images obtained with the capacitance wire-mesh sensor: (a) o/w H (U_{ws} = 2.5 m/s, U_{os} = 0.9 m/s); (b) o/w NH (U_{ws} = 1.5 m/s, U_{os} = 0.9 m/s); (c) Do/w & Dw/o (U_{ws} = 1.0 m/s, U_{os} = 0.9 m/s).

data suggest that a thin water film is probably surrounding a mixture of oil in water in the dispersed flow investigated in this study. The water film might be related to the physical mechanism of drag reduction in fully dispersed flow at high mixture Reynolds numbers. More details concerning the volume fraction results can be seen in Rodriguez et al.[33]

Modeling

Considering the literature, one may expect that the two-phase dispersed flow at high mixture velocities and Reynolds numbers ($30{,}000 < Re_m < 120{,}000$) should behave as a homogeneous no-slip mixture. However, results show significant slip ratio between the phases in the dispersed flow studied. The slip ratio, s, is defined as

$$s = \frac{\frac{\varepsilon_w}{\varepsilon_o}}{\frac{C_w}{C_o}} = \frac{V_o}{V_w} \tag{7}$$

where ε_o and ε_w stand for *in situ* volume fractions, V_o and V_w *in situ* velocities and C_o and C_w the cuts of oil and water, respectively. The oil and water cuts can be also denoted by

$$C_o = \frac{Q_o}{Q_w + Q_o} = \frac{U_{os}}{U_{ms}} \tag{8}$$

$$C_w = \frac{Q_w}{Q_o + Q_w} = \frac{U_{ws}}{U_{ms}} \tag{9}$$

Where Q_w and Q_o are water and oil volume flow rates, respectively.

Accordingly to Eq. 7, the slip ratio s is >1 when oil is the fastest flowing phase. Slip ratio was found to be >1 for all experimental points (Table 2), showing that oil is always flowing faster than water, even in the homogeneous dispersed flow (o/w H). A possible explanation may be the presence of a thin annular water film between the pipe wall and the homogenous mixture of oil in water. This article proposes a phenomenological model, analogous to the idea of the core-annular flow model[9,10,23,24] to explain the occurrence of the drag reduction detected in this study. In core-annular flow the two-phase pressure gradient is usually of the same order of that of the related single-phase water flow, similarly to what was observed in the oil-water dispersed flow investigated.

Film model

The model is based on the idea that there is a thin film of water adjacent to the pipe wall surrounding an axisymmetric core that is constituted of a homogeneous oil-water mixture. Accordingly, the water fraction (ε_w) can be split into the water-film fraction ($\varepsilon_{w,f}$) and fraction of water in the core mixture ($\varepsilon_{w,m}$)

$$\varepsilon_w = \frac{U_{ws}}{V_w} = \varepsilon_{w,f} + \varepsilon_{w,m} = \frac{U_{ws,f}}{V_{w,f}} + \frac{U_{ws,m}}{V_{w,m}} \tag{10}$$

where $U_{ws,f}$ and $U_{ws,m}$ are the superficial velocities and $V_{w,f}$ and $V_{w,m}$ are the *in situ* velocities of the water film and water in the core mixture, respectively. The oil fraction is defined as

$$\varepsilon_o = \frac{U_{os}}{V_o} \tag{11}$$

and the water flow rate can be divided in

$$Q_w = Q_{w,f} + Q_{w,m} = U_{ws,f}A + U_{ws,m}A = U_{ws}A \tag{12}$$

where $Q_{w,f}$ and $Q_{w,m}$ are water-film flow rate and water flow rate of the core mixture, respectively, and A is the cross-sectional area of the pipe. Combining Eqs. 7–12, the slip ratio becomes

$$s = \frac{\frac{\varepsilon_{w,f}+\varepsilon_{w,m}}{\varepsilon_o}}{\frac{C_w}{C_o}} = \frac{U_{ws,f}V_o}{V_{w,f}\left(U_{ws,f} + U_{ws,m}\right)} + \frac{U_{ws,m}V_o}{V_{w,m}\left(U_{ws,f} + U_{ws,m}\right)} \tag{13}$$

At this point, some assumptions are needed:

1. The superficial water-film velocity is assumed to be much lower than the superficial velocity of water of the core mixture, i.e., $U_{ws,f} << U_{ws,m}$; so, $U_{ws,m}$ tends to the superficial velocity of water, U_{ws}.

2. Due to the no-slip boundary condition at the pipe wall, the *in situ* water-film velocity ($V_{w,f}$) is expected to be lower than the *in situ* velocity of water in the core mixture ($V_{w,m}$); therefore, $V_o > V_w$. Notice that slip ratio (Eq. 7 and Table 2) is a function of the *in situ* water velocity (V_w), which in turn is a function of the water-film velocity and velocity of water in the core mixture.

3. The *in situ* velocity of water in the core mixture, $V_{w,m}$, is assumed to be equal to the *in situ* velocity of oil, V_o. In other words, it is assumed that the oil-water core mixture flows as a homogeneous no-slip mixture uniformly distributed over the cross-section of the pipe (excluding the annular section occupied by the water film); a turbulent flow of high-intensity turbulence would justify the assumption. Hence, the second term of the RHS of Eq. 13 tends to 1.

Therefore, the following expression for slip ratio is suggested

$$s = \frac{V_o}{V_{w,f}}\left(\frac{Q_{w,f}}{Q_w}\right) + 1 \tag{14}$$

where s is a function of two unknowns parameters, $V_{w,f}$ and $Q_{w,f}$, *i.e.*, $s = s\ (V_{w,f}, Q_{w,f})$.

The proposed film model presupposes the existence of a laminar flow of an annular water film, which would explain both the detected drag reduction and the measured slip ratio. To estimate the water-film thickness a few additional assumptions are needed:

4. The water-film thickness is assumed to be very thin; then, the radial velocity component is equal to zero.

5. The azimuthal velocity component is equal to zero; hypothesis of axisymmetry.

These assumptions are similar to those adopted for core-annular flow.[10] Accordingly, the water-film velocity profile can be expressed as

$$u_{w,f}(r) = \frac{-(dp/dx)_m}{4\mu_w}(R^2 - r^2) + \frac{\rho_w g_z}{4\mu_w}(R^2 - r^2) + (\rho_m - \rho_w)g_z\frac{R_2^2}{2\mu_w}\ln\left(\frac{R}{r}\right) \tag{15}$$

where $(dp/dx)_m$ is the mixture pressure gradient (Eq. 4), r is the radial coordinate, R_2 is the radius of the oil-water mixture, R is the radius of the pipe, ρ_w is the water density, ρ_m is the mixture density (Eq. 2), μ_w is the water viscosity (see 'Friction factor and effective viscosity estimates' section) and g_z is the gravity component in the axial direction ($g_z = g \sin\theta$ and θ is

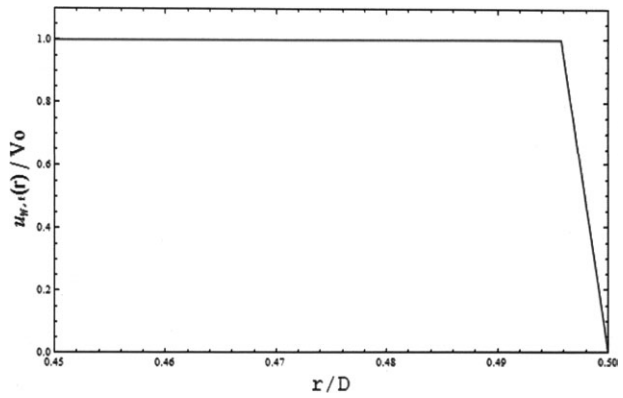

Figure 9. Dimensionless water-film velocity profile as a function of the radial coordinate.

the inclination angle from the horizontal).

Equation 15 is numerically solved with the boundary condition $u_{w,f}(R_2) = V_o$ and the data of $(dp/dx)_m$ (Table 2) to obtain the radius of the oil-water mixture, R_2. Figure 9 shows the water-film velocity profile (Eq. 15) normalized with respect to the *in situ* oil velocity as a function of the radial coordinate normalized by the pipe diameter. The water-film velocity reaches the velocity of the homogeneous mixture, V_o, at approximately $r/D = 0.496$ for $U_{ws,f} = 0.03$ m/s and $(U_{os} + U_{ws,m}) = 3.17$ m/s.

The water-film flow rate is then obtained by replacing the known value of R_2 in the following equation

$$Q_{w,f} = \int_{R_2}^{R} u_{w,f}(r) 2\pi r dr \tag{16}$$

Finally, the water-film velocity is calculated by

$$V_{w,f} = \frac{Q_{w,f}}{\pi(R^2 - R_2^2)} \tag{17}$$

Equation 14 can then be applied for obtaining the theoretical slip ratio. A comparison between slip-ratio data and model predictions can be seen in Figure 10.

The data of Rodriguez and Oliemans[28] corresponding to dispersed flow can also be seen in Figure 10. Those authors used 82.8-mm-i.d. 15.5 m length steel pipe, oil (viscosity of 7.5 mPa s and density of 830 kg/m^3) and brine (viscosity of 0.8 mPa s and density of 1060 kg/m^3) as test fluids. The predicted values of slip ratio agree quite well with experimental data for both data sets, with a maximum deviation of about 10%. Qualitatively, there is a slight underestimation at higher values of slip. Considering the simplicity of the proposed model, the results are promising and corroborate the hypothesis of the existence of a laminar water film.

In addition, the water-film Reynolds number is defined as

$$Re_f = \frac{\rho_w V_{w,f}(2e)}{\mu_w} \tag{18}$$

where the water film thickness is defined as $e = R - R_2$.

Mixture laminar sublayer

An analogy with single-phase turbulent pipe flow is adopted to define the effective laminar sublayer of a homogeneous two-phase mixture. The shear stress at the wall, τ_w, is calculated as a function of the two-phase pressure gradient

$$\tau_w = -\left(\frac{R}{2}\right)\left(\frac{\partial p}{\partial x}\right)_m \tag{19}$$

The mixture friction velocity is calculated as

$$V_{frict,m} = \left(\frac{\tau_w}{\rho_m}\right)^{1/2} \tag{20}$$

and the thickness of the effective mixture laminar sublayer is given by

$$\delta_{sub,m} = \frac{5\left(\frac{\mu_w}{\rho_m}\right)}{V_{frict,m}} \tag{21}$$

Note that for water cuts higher that 40% ($C_w > 0.40$) the effective viscosity of the dispersion of oil in water can be assumed to be equal to the viscosity of pure water (see Figure 5 and Guet et al.[36]).

Results

The computed water-film thickness ranged from 0.12 to 0.33 mm. The water-film thickness normalized with respect to the mixture laminar sublayer thickness can be seen as a function of slip ratio in Figure 11. It is not observed significant variation of the dimensionless water-film thickness for all flow patterns observed by Rodriguez et al.,[33] a slight trend of increasing with slip ratio may be inferred. The water-film is four to five times as thick as the mixture laminar sublayer.

Figure 12 shows the dimensionless water-film thickness as a function of the water-film Reynolds number (Eq. 18). There is clearly a linear relation between the dimensionless water-film thickness and the Reynolds number of the water film for all flow patterns observed by Rodriguez et al.[33] It increases with increasing the Reynolds number. The relatively low Reynolds numbers suggest that the water-film flow is in laminar regime, in accordance with the proposed model. For instance, in core-annular flow the critical Reynolds number is around 1500 (Joseph and Renardy[10]).

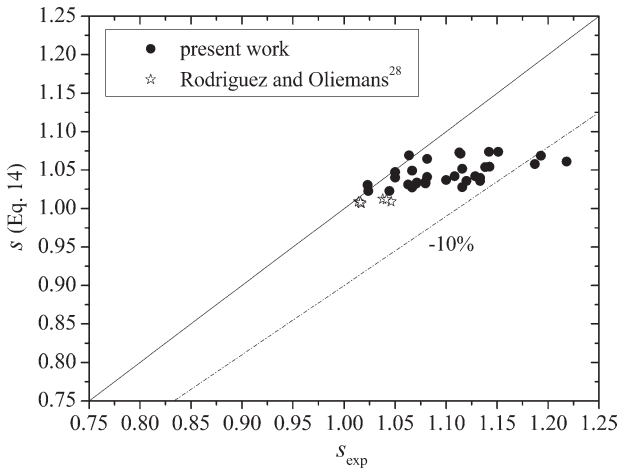

Figure 10. Comparison between the slip-ratio data, s_{exp}, and predictions of the present model, s (Eq. 14).

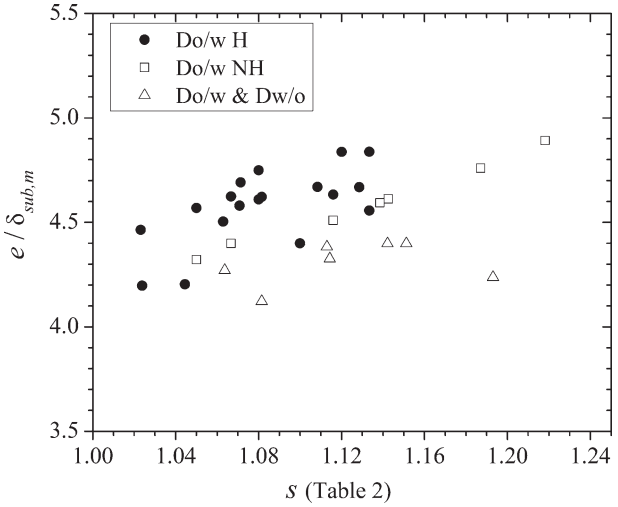

Figure 11. Dimensionless water-film thickness as a function of slip ratio.

The DRP factor can be observed as a function of the water-film Reynolds number for all experimental points in Figure 13. The data of Rodriguez and Oliemans[28] can also be seen in Figure 13. It can be noticed that the DRP tends to be lower with increasing the water-film Reynolds number. Inspection of Figures 12 and 13 suggests that an increase of the dimensionless water-film thickness leads to stronger drag reduction. An increase of the water-film thickness represents an increase of the cross-sectional area for the water-film flow, which in turn leads to lower wall shear stress (refer to Figure 9).

Overall, the results suggest that the presence of a laminar water film surrounding a turbulent core of mixture of oil in water could explain the drag reduction and slip ratio measured in this study. The phenomenological model, off course, is based on some important simplifications. The most important is the idea that the core of oil-water dispersion is axisymmetric. Although one can argue that the studied flows are dominated by turbulence ($30{,}000 < Re_m < 120{,}000$) this is not absolutely true, as can be seen in Figures 6–8. Therefore, the predicted water-film thickness is actually an axisymmetric equivalent of the average water film thickness. The model would perhaps be more suitable to vertical flow.

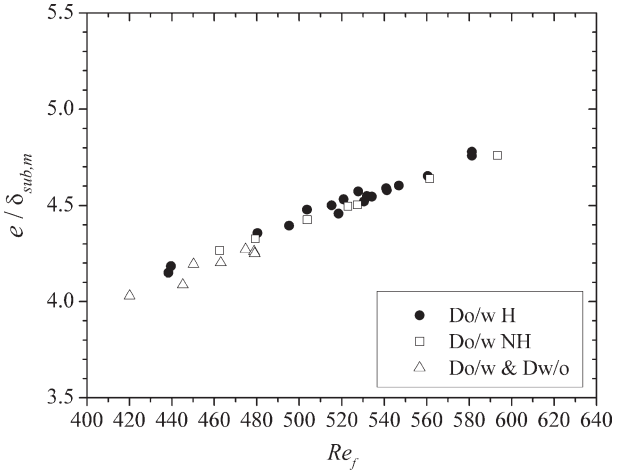

Figure 12. Dimensionless water-film thickness as a function of the water-film Reynolds number.

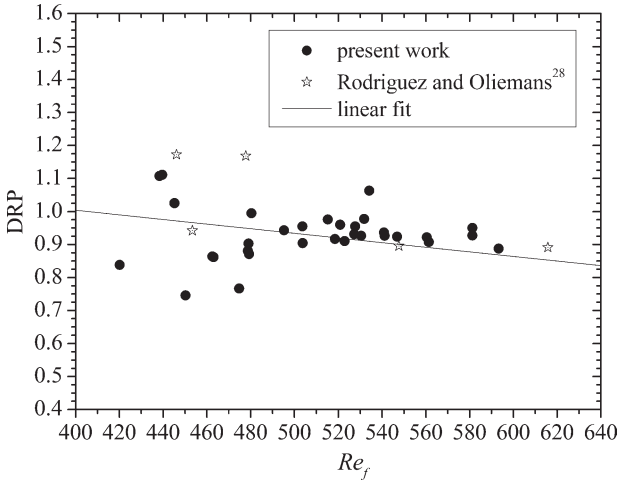

Figure 13. DRP factor as a function of the water-film Reynolds number; solid line represents linear fit of data.

Conclusions

New two-phase pressure gradient, volume fraction and phase distribution data have been used for the study of DRP in dispersed viscous oil-water flow. A measured reduction of up to 25% of two-phase pressure gradient with respect to single-phase water pressure-gradient at the same mixture velocity confirmed the occurrence of the phenomenon. Mixture friction factor and effective mixture viscosity were also important indicators of the occurrence of drag reduction. The results suggest that it occurs at high mixture Reynolds numbers ($30{,}000 < Re_m < 120{,}000$) and for oil fractions between 10 and 45%. Phase distribution diagrams that were obtained via capacitive wire-mesh sensing showed the presence of a higher amount of water near to the pipe wall. Based on experimental evidence, a phenomenology is proposed to explain drag reduction in dispersed oil-water pipe flow. It is suggested that a laminar flow of a thin water film surrounding a turbulent flow of a core of oil-water dispersion would explain both the drag reduction and the significant slip ratio observed.

A simple phenomenological model based on the laminar water-film hypothesis (Perfect Core-Annular Flow model) is proposed and used to numerically compute the water-film thickness. A new expression for slip ratio based on the film model was deduced and its predictions agreed quite well with the data obtained in this study and also from the literature (maximum deviation of 10%). An analogy with single-phase turbulent pipe flow was adopted to define the effective laminar sublayer of a homogeneous mixture. According to the model, the predicted water-film thickness would be an axisymmetric equivalent of the average laminar water-film thickness. The water film is four to five times as thick as the mixture laminar sublayer, which suggests that it could be acting as a lubricating film. There is a linear relation between the dimensionless water-film thickness and the water-film Reynolds number. It increases with increasing the Reynolds number. The relatively low water-film Reynolds numbers ($400 < Re_f < 600$) suggest that the water-film flow is in laminar regime, in accordance with the proposed model. According to the model, an increase of the water-film thickness leads to stronger drag reduction, which can be explained by an increase of the cross-sectional area for the water-film flow, which in turn leads to lower wall shear stress.

The complexity of the DRP is clearly a ripe field for further investigation. The study should be enhanced by the obtaining of more detailed experimental data on oil-water dispersed flow and taking into account the role of the pipe material and especially wetting properties. The development of experimental techniques aiming to the detailed characterization of the water film, as measurement of its thickness, velocity profiles in the cross-section, in the water film and core, measurements with high spatial and temporal resolutions of phase distribution adjacent to the pipe wall, is of major importance for any subsequent analysis, although it is not trivial. Measurements with single-beam gamma densitometry and micro-PIV are a suggestion. The dynamics that lead to the topological arrangement of a core mixture surrounded by a water film of course need yet to be explained. Further theoretical investigation on the hydrodynamic stability of such flow pattern is in order. Nevertheless, the measurements carried out and data offered in this article represent a step forward and support the attempt of explaining the drag-reduction phenomenon in dispersed flows with significant slip ratio.

Acknowledgments

The authors are grateful to CAPES (Coordenação de Aperfeiçoamento de Pessoal de Nível Superior) and FAPESP (Fundação de Amparo à Pesquisa do Estado de São Paulo, proc. 2008/06922-9) for the financial support given to this research and also to Dresden-Rossendorf Research Center (Germany) for the contribution in the experimental work. I.H. Rodriguez thank Dresden-Rossendorf Research Center (Germany) and Dr. Uwe Hampel for providing part of the financial support for her student internship.

Literature Cited

1. Pal R. Pipeline flow of unstable and surfactant stabilized emulsions. *AIChE J*. 1993;39:1754–1764.
2. Pal R. Viscosity-concentration equation for emulsions of nearly spherical droplets. *J Colloid Interface Sci*. 2000;231:168–175.
3. Nädler M, Mewes D. Flow induced emulsification in the flow of two immiscible liquids in horizontal pipes. *Int J Multiphase Flow*. 1997;23:55–68.
4. Angeli P, Hewitt GF. Pressure gradient in horizontal liquid–liquid flows. *Int J Multiphase Flow*. 1998;24:1183–1203.
5. Lovick J, Angeli P. Experimental studies on the dual continuous flow pattern in oil–water flows. *Int J Multiphase Flow*. 2004;30:139–157.
6. Ioannou K, Nydal O, Angeli P. Phase inversion in dispersed liquid–liquid flows. *Exp Therm Fluid Sci*. 2005;29:331–339.
7. Lum JYL, Al-Wahaibi T, Angeli P. Upward and downward inclination oil–water flows. *Int J Multiphase Flow*. 2006;32:413–435.
8. Pal R. Mechanism of Turbulent Drag Reduction in Emulsions and Bubbly Suspensions. *Ind Eng Chem Res*. 2007; 618–622.
9. Oliemans R, Ooms G. Core-annular flow of oil and water through a pipeline. In: Hewitt GF, Delhaye JM, Zuber N (Eds.), Multiphase Science and Technology. 1986;2:427–476.
10. Joseph D, Renardy Y. *Fundamentals of Two-Fluid Dynamics: Part II: Lubricated Transport, Drops and Miscible Liquid*. New York: Springer-Verlag, 1993.
11. Russel T, Charles M. The effect of the less viscous liquid in the laminar flow of two-immiscible liquids. *Can J Chem Eng*. 1959;37:18–24.
12. Charles M, Govier G, Hodgson G. The horizontal pipeline flow of equal density of oil–water mixtures. *Can J Chem Eng*. 1961;39:27–36.
13. Ooms G. The hydrodynamic stability of core-annular flow of two ideal liquids. *Appl Sci Res*. 1972;26:147–158.
14. Ooms G, Segal A, Vanderwees AJ, Meerhoff R, Oliemans RVA. A theoretical model for core-annular flow of a very viscous oil core and a water annulus through a horizontal pipe. *Int J Multiphase Flow*. 1984;10:41–60.
15. Oliemans R. The lubricating-film model for core-annular flow, Ph.D. thesis, Delft University of Technology, 1986.
16. Joseph D, Renardy Y, Renardy M. Instability of the flow of 2 immiscible liquids with different viscosities in a pipe. *J Fluid Mech*. 1984;141: 309–317.
17. Feng J, Huang P, Joseph D. Dynamic simulation of the motion of capsules in pipelines. *J Fluid Mech*. 1995;286:201–227.
18. Bai R. Traveling waves in a high viscosity ratio and axisymmetric core annular flow, Ph.D. thesis, University of Minnesota, 1995.
19. Bai R, Kelkar K, Joseph DD. Direct simulation of interfacial waves in a high-viscosity-ratio and axisymmetric core–annular flow. *J Fluid Mech*. 1996;327:1.
20. Bai R, Joseph DD. Steady flow and interfacial shapes of a highly viscous dispersed phase. *Int J Multiphase Flow*. 2000;26:1469–1491.
21. Rodriguez OMH, Bannwart AC. Experimental study on interfacial waves in vertical core flow. *J Pet Sci Eng*. 2006;54:140–148.
22. Rodriguez OMH, Bannwart AC. Analytical model for interfacial waves in vertical core flow. *J Pet Sci Eng*. 2006;54:173–182.
23. Rodriguez OMH, Bannwart AC, carvalho CHM de. Pressure loss in core-annular flow: modeling, experimental investigation and full-scale experiments. *J Pet Sci Eng*. 2009;65:67–75.
24. Rodriguez OMH, Bannwart AC. Stability analysis of core-annular flow and neutral stability wave number. *AIChE J*. 2008;54:20–31.
25. Yang W, Spink D, Gamio J, Beck M. Sensitivity distributions of capacitance tomography sensors with parallel field excitation. *Meas Sci Technol*. 1997;8:562–569.
26. Ismail I, Gamio JC, Bukhari SFA, Yang WQ. Tomography for multi-phase flow measurement in the oil industry. *Flow Meas Instrum*. 2005;16:145–155.
27. Tjugum SA, Hjertaker BT, Johansen GA. Multiphase flow regime identification by multibeam gamma-ray densitometry. *Meas Sci Technol*. 2002;13:1319–1326.
28. Rodriguez OMH, Oliemans RVA. Experimental study on oil–water flow in horizontal and slightly inclined pipes. *Int J Multiphase Flow*. 2006;32:323–343.
29. Kumara W a S, Halvorsen BM, Melaaen MC. Single-beam gamma densitometry measurements of oil–water flow in horizontal and slightly inclined pipes. *Int J Multiphase Flow*. 2010;36:467–480.
30. Kumara W a S, Elseth G, Halvorsen BM, Melaaen MC. Comparison of particle image velocimetry and laser Doppler anemometry measurement methods applied to the oil–water flow in horizontal pipe. *Flow Meas Instrum*. 2010;21:105–117.
31. Prasser HM, Bottger A, Zschau J. A new electrode-mesh tomograph for gas–liquid flows. *Flow Meas Instrum*. 1998;9:111–119.
32. Da Silva MJ, Schleicher E, Hampel U. Capacitance wire-mesh sensor for fast measurement of phase fraction distributions. *Meas Sci Technol*. 2007;18:2245–2251.
33. Rodriguez IH, Yamaguti HKB, Castro MS de, Da Silva MJ, Rodriguez OMH. Slip ratio in dispersed viscous oil–water pipe flow. *Exp Therm Fluid Sci*. 2011;35:11–19.
34. Brauner N, Ullmann A. Modeling of phase inversion phenomenon in two-phase pipe flows. *Int J Multiphase Flow*. 2002;28:1177–1204.
35. Wallis GB. *One-Dimensional Two-Phase Flow*. New York: McGraw-Hill, 1969.
36. Guet S, Rodriguez O, Oliemans R, Brauner N. An inverse dispersed multiphase flow model for liquid production rate determination. *Int J Multiphase Flow*. 2006;32:553–567.

Manuscript received May 11, 2011, and revision received Sept. 15, 2011.